J M M
Journal of Mechanics and MEMS
*Special Issue dedicated to Prof. K Y Ye edited by Z M Ye, P Liu and B Sun*

ISSN: 0974-8407

9(2) 2017: pp. 299-312

# SPECIAL ELLIPTIC HOLE ELEMENTS OF TREFFTZ FEM IN STRESS CONCENTRATION ANALYSIS

**Qing-Hua Qin[1] and Xiao-Qiao He[2]**

**ABSTRACT**

The purpose of this paper is to develop a special Trefftz element model for analyzing the influence of holes on the contact pressure distribution in 2D contact problems. A rotated mapping function is introduced into the conventional conformal transformation in order to make the new special hole element applicable to an element with arbitrarily oriented elliptical hole. The developed special Trefftz element model is then used to analyze stress concentration due to a number of arbitrarily oriented elliptical holes embedded in a frictionless unilateral contact structure composed of an elastic rectangular punch and an elastic foundation. The study shows that the number of Trefftz functions used in a special element should be approximately equal to the total degrees of freedom of the element. A numerical example of an elastic rectangular punch pressed on an elastic foundation with arbitrarily oriented holes is considered to assess the effectiveness and applicability of the new special element. The numerical results are found to be in good agreement with the predictions by the commercial finite element (FE) software package ABAQUS, although the number of elements used here is much less than those used in the ABAQUS.

***Keywords***: Trefftz function, Finite element method, Contact mechanics, hole element

## 1. INTRODUCTION

Contacts between two structures with holes or cut-outs occur frequently in the engineering applications. It should be underlined that such holes or cut-outs may cause significant stress concentration near the hole boundary. In the conventional FE analysis, a troublesome mesh refinement in the vicinity of each hole needs to be conducted. This gives rise to great difficulty in constructing conventional FE mesh, especially in the case of multiple holes or cut-outs embedded in contacting bodies.

As a highly efficient and well established computational tool, hybrid Trefftz (HT) finite element method (FEM), initiated about three decades ago [1], has attracted considerable attention in practical engineering. This method preserves the advantages of conventional FEM and boundary element method (BEM) and avoids some of their drawbacks [2, 3]. The common characteristics is that the trial functions (so called Trefftz functions) exactly satisfy, *a priori*, the governing differential equations, and for special purpose elements, they should also satisfy boundary conditions on influential critical boundary portions (the hole surface here). In order to reduce the time-consuming and tedious process involved in generating refined mesh around a hole, many kinds of special finite elements have been developed in recent years. A remarkable research was first made by Piltner [4], who proposed the formulation in an example of an ellipse that was mapped onto a circle with the aid of conformal transformation, but the ellipse there is limited to be oriented horizontally. Consequently, a series of attempts were undertaken by Zhao and Shan [5], Chen [6], ZieliDski [7], and Zeng *et al.* [8].

As stated in Ref [9], on the other hand, HT FEM is particularly well suited for contact problems. In this study, an in-house developed HT FE analysis program [9] has been adopted to investigate the different facets of the research. The code is suitable for two-dimentional (2D) elastic contact problems including receding, conforming and advancing situations. Details of the algorithm have been discussed by Wang *et al.* [9] elsewhere. A rotated

1. Department of Engineering, Australian National University, Canberra, ACT 0200, Australia
2. Department of Building and Construction, City University of Hong Kong, Hong Kong

mapping function is introduced into the conventional conformal transformation in order to make the new special hole element applicable to an element with arbitrarily oriented elliptical hole. Based on the developed special element model, a numerical example of an elastic rectangular punch pressed on an elastic foundation with arbitrarily oriented holes is considered to assess the effectiveness and applicability of the new special element. Comparison of the present results with the predictions by the commercial FE software package ABAQUS has been made and a good agreement is observed, although the number of elements used here is much less than those used in the ABAQUS.

## 2. SPECIAL TREFFTZ HOLE ELEMENT

### 2.1. Element Formulation

The HT FE model used here is based on simultaneous use of two independent displacement fields (Fig. 1) [2]
(a) A non-conforming 'Trefftz' field

$$\mathbf{u}_e = \breve{\mathbf{u}}_e + \sum_{j=1}^{m} \mathbf{N}_{ej} c_{ej} = \breve{\mathbf{u}}_e + \mathbf{N}_e \mathbf{c}_e \text{ in } \Omega_e, \tag{1}$$

being defined over intra-element domain, where $c_{ej}$ stands for undetermined coefficients and $\breve{\mathbf{u}}_e$ and $\mathbf{N}_{ej}$ are, respectively, the particular and homogeneous solutions to the governing differential equations [2].

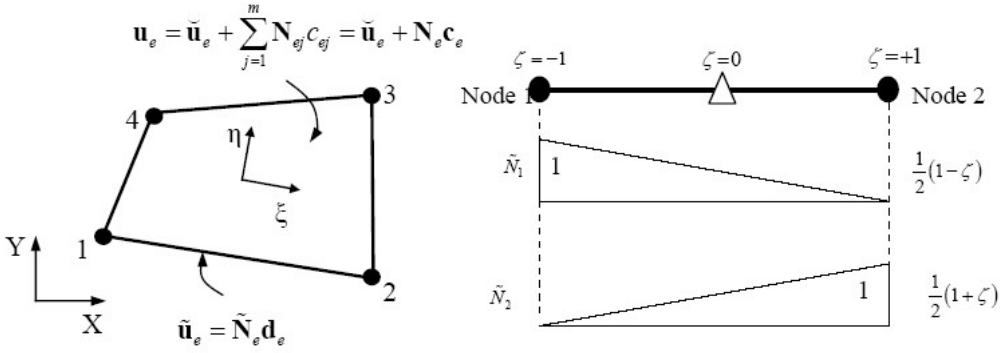


**Figure 1: The Configuration of the T-element Model**

(b) An exactly and minimally conforming auxiliary frame field

$$\tilde{\mathbf{u}}_e = \tilde{\mathbf{N}}_e \mathbf{d}_e \text{ on } \Gamma_e \tag{2}$$

being independently assumed along the element boundary in terms of nodal degrees of freedom $\mathbf{d}_e$, where $\Gamma_e = \Gamma_{eu} \cup \Gamma_{et} \cup \Gamma_{eI}$, $\Gamma_{eu} = \Gamma_u \cap \Gamma_e$, $\Gamma_{et} = \Gamma_t \cap \Gamma_e$, and $\Gamma_{eI}$ is the inter-element boundary, $\tilde{\mathbf{N}}_e$ are the shape functions (frame functions) defined in the customary way as in conventional FEM. The tilde above a symbol in Eq (2) allows the two fields to be distinguished.

The corresponding stress field

$$\boldsymbol{\sigma}_e = \breve{\boldsymbol{\sigma}}_e + \sum_{j=1}^{m} \mathbf{T}_{ej} c_{ej} = \breve{\boldsymbol{\sigma}}_e + \mathbf{T}_e \mathbf{c}_e \tag{3}$$

as well as the boundary tractions

$$\mathbf{t}_e = \breve{\mathbf{t}}_e + \sum_{j=1}^{m} \mathbf{Q}_{ej} c_{ej} = \breve{\mathbf{t}}_e + \mathbf{Q}_e \mathbf{c}_e \tag{4}$$

can be readily deduced from $\sigma_e = \mathbf{D}\mathbf{L}^{\mathrm{T}}\mathbf{u}_e$ and $\mathbf{t}_e = \mathbf{A}\boldsymbol{\sigma}_e$ respectively, where $\mathbf{L}$ is the differential operator matrix, $\mathbf{D}$ contains elastic constants and $\mathbf{A}$ contains components of a unit normal to the element boundary $\Gamma_e$ (see [2] for the detailed expressions of $\mathbf{L}$, $\mathbf{D}$, and $\mathbf{A}$)

The HT FE formulation for 2D elastic problems may be obtained by means of the following modified variational principle [2]

$$\Pi_m = \Pi_c - \sum_e \left[ \int_{\Gamma_{et}} \left( \mathbf{t}_e - \bar{\mathbf{t}}_e \right)^{\mathrm{T}} \tilde{\mathbf{u}}_e \, \mathrm{d}\Gamma + \int_{\Gamma_{el}} \mathbf{t}_e^{\mathrm{T}} \tilde{\mathbf{u}}_e \, \mathrm{d}\Gamma \right] \tag{5}$$

where $\Pi_c$ is the total complementary energy [2], the overhead bar is used to designate specified values.

Applying the stationary condition to Eq (5) straightforwardly leads to the symmetric element stiffness equation

$$\mathbf{K}_e \, \mathbf{d}_e = \mathbf{P}_e \tag{6}$$

where

$$\mathbf{K}_e = \mathbf{G}_e^{\mathrm{T}} \mathbf{H}_e^{-1} \mathbf{G}_e \tag{7}$$

$$\mathbf{P}_e = \mathbf{G}_e^{\mathrm{T}} \mathbf{H}_e \mathbf{h}_e - \mathbf{g}_e \tag{8}$$

Here the auxiliary matrices $\mathbf{H}_e$, $\mathbf{G}_e$, $\mathbf{h}_e$ and $\mathbf{g}_e$ are explicitly expressed as

$$\mathbf{H}_e = \int_{\Gamma_e} \mathbf{Q}_e^{\mathrm{T}} \mathbf{N}_e \, \mathrm{d}\Gamma = \int_{\Gamma_e} \mathbf{N}_e^{\mathrm{T}} \mathbf{Q}_e \, \mathrm{d}\Gamma \tag{9}$$

$$\mathbf{G}_e = \int_{\Gamma_e} \mathbf{Q}_e^{\mathrm{T}} \tilde{\mathbf{N}}_e \, \mathrm{d}\Gamma \tag{10}$$

$$\mathbf{h}_e = \frac{1}{2} \int_{\Gamma_e} \left( \mathbf{N}_e^{\mathrm{T}} \breve{\mathbf{t}} + \mathbf{Q}_e^{\mathrm{T}} \breve{\mathbf{u}}_e \right) \mathrm{d}\Gamma + \frac{1}{2} \iint_{\Omega_e} \mathbf{N}_e^{\mathrm{T}} \bar{\mathbf{b}}_e \, \mathrm{d}\Omega \tag{11}$$

$$\mathbf{g}_e = \int_{\Gamma_e} \tilde{\mathbf{N}}_e^{\mathrm{T}} \breve{\mathbf{t}}_e \, \mathrm{d}\Gamma - \int_{\Gamma_{et}} \tilde{\mathbf{N}}_e^{\mathrm{T}} \bar{\mathbf{t}}_e \, \mathrm{d}\Gamma \tag{12}$$

in which $\bar{\mathbf{b}}_e$ stands for the body force.

### 2.2. Special Purpose Trefftz Functions

A key step in constructing an accurate special purpose element for a hole region is to find a special set of trail functions which reflect the local stress concentration characteristics. To achieve this, the Muskhelishvili's complex variable formulation [10] is utilized herein. It should be mentioned that the special purpose element presented here is an extension of Piltner's element[4] by introducing a rotated mapping function and using different terms of Trefftz functions. Through use of the rotated mapping function the limitation of ellipse in horizontal direction in Piltner's element is removed. The number of Trefftz functions *m* for elliptical hole elements is suggested here to be equal to the number of elemental degrees of freedom, which is different from Piltner's recommendation, as his recommendation on the choice of terms of Trefftz functions can accurately represent an element with circular hole only. The derivation of special Trefftz function can be carried out by using following expressions of displacements and stresses [4]

$$2G(u + iv) = \kappa \phi(z) - z \overline{\dot{\phi}}(z) - \overline{\psi}(z) \tag{13}$$

$$\sigma_{xx} + i\sigma_{xy} = \dot{\phi}(z) + \overline{\dot{\phi}}(z) - z \overline{\ddot{\phi}}(z) - \overline{\dot{\psi}}(z) \tag{14}$$

$$\sigma_{yy} - i\sigma_{xy} = \dot{\phi}(z) + \overline{\dot{\phi}}(z) + z \overline{\ddot{\phi}}(z) + \overline{\dot{\psi}}(z) \tag{15}$$

where $z = x + iy$, $i = \sqrt{-1}$, $\phi(z)$ and $\psi(z)$ are two analytical functions, $G = E / 2(1 + \mu)$, $\kappa = (3 - \mu)/(1 + \mu)$, $E$ and $\mu$ are, respectively, Young's modulus and Poisson's ratio, $\dot{(\,)}$ denotes differentiation with respect to $z$ and $\overline{(\,)}$ represents complex conjugate. The boundary conditions can be given in the complex form as

$$\kappa \phi(z) - z \overline{\dot{\phi}}(z) - \overline{\psi}(z) = 2G(\bar{u} + i\bar{v}) \quad \text{on } \Gamma_u \tag{16}$$

$$\phi(z) + z \overline{\dot{\phi}}(z) + \overline{\psi}(z) = i \int (\bar{t}_x + i\bar{t}_y) \mathrm{d}\Gamma \quad \text{on } \Gamma_t \tag{17}$$

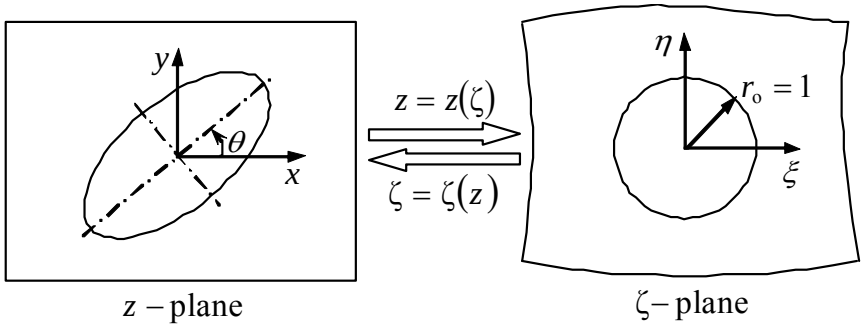


**Figure 2: Conformal Mapping for Constructing Special Hole Element**

Due to the fact that Piltner's hole element is based on the horizontal conformal transformation, it is tedious to treat structures with holes in arbitrary direction. To bypass this difficulty, a rotated mapping function

$$\wp(\theta) = e^{i\theta} \tag{18}$$

is introduced into the horizontal conformal transformation as

$$z = f(\zeta) = \wp(\theta)c(\zeta + m\zeta^{-1}) = ce^{i\theta}(\zeta + m\zeta^{-1}) \tag{19}$$

where $c = (a + b) / 2$, $m = (a - b) / (a + b)$, $a$ and $b$ are, respectively, the semi-major axis and semi-minor axis, $\theta$ is the angle between the semi-major axis and $x$ axis (Fig. 2).

Substituting the inverse transformation

$$\zeta = f^{-1}(z) = \frac{1}{2ce^{i\theta}}\left(z \pm \sqrt{z^2 + 4c^2 m e^{i2\theta}}\right) \tag{20}$$

into Eqs (13)-(15) produces the displacements and stresses in the $\zeta$-plane as:

$$2G\left(u_x + iu_y\right) = \kappa\phi - f\frac{\overline{\dot{\phi}}}{\dot{f}} - \overline{\psi} \tag{21}$$

$$\sigma_{xx} - i\tau_{xy} = \frac{\dot{\phi}}{\dot{f}} + \frac{\overline{\dot{\phi}}}{\overline{\dot{f}}} - \frac{\overline{f}\left(\dot{f}\ddot{\phi} - \ddot{f}\dot{\phi}\right)}{\dot{f}^3} - \frac{\dot{\psi}}{\dot{f}} \tag{22}$$

$$\sigma_{yy} - i\tau_{xy} = \frac{\dot{\phi}}{\dot{f}} + \frac{\overline{\dot{\phi}}}{\overline{\dot{f}}} + \frac{\overline{f}\left(\dot{f}\ddot{\phi} - \ddot{f}\dot{\phi}\right)}{\dot{f}^3} + \frac{\dot{\psi}}{\dot{f}} \tag{23}$$

Here, the sign in Eq (20) is chosen in a similar way to that in Ref [4].

The transformed boundary conditions along the hole surface can be expressed as

$$\psi(\zeta) = \kappa\overline{\phi} - \overline{f}\frac{\dot{\phi}}{\dot{f}} - 2G\left(\overline{u + iv}\right) \text{ on } \Gamma'_u \tag{24}$$

$$\psi(\zeta) = -\overline{\phi} - \overline{f}\frac{\dot{\phi}}{\dot{f}} - i\overline{\int\left(\overline{t}_x + i\overline{t}_y\right)\,\mathrm{d}\Gamma} \text{ on } \Gamma'_t \tag{25}$$

In general, it is impossible to find a formulation for $\phi(\zeta)$ and $\psi(\zeta)$ in closed form for arbitrary geometry and boundary conditions. Following the way of Piltner [4], we can expanded the two holomorphic functions in the general expressions of elasticity solutions into two complex Laurent series respectively as follows

$$\phi(\zeta) = \sum_{j=-N}^{M} c_j \zeta^j \tag{26}$$

$$\psi(\zeta) = -\sum_{j=-N}^{M}\left[\overline{c}_j \zeta^{-j} + c_j j\frac{\zeta^{j-2} + m\zeta^j}{e^{i2\theta}\left(1 - m\zeta^{-2}\right)}\right] \tag{27}$$

where $c_j = a_j + ib_j$ are complex coefficients, $M$ and $N$ are the upper and lower limits of the Laurent series and $M$ is generally set to be $N$ for symmetry, Eq (27) is obtained according to the traction-free condition along the hole boundary. Therefore, the displacement and stress fields are given in the following form

$$2G\left(u_x + iu_y\right) = \sum_{j=-N}^{M}\left[\left(\varsigma_1 - \varsigma_2\right)a_j + i\left(\varsigma_1 + \varsigma_2\right)b_j\right] \tag{28}$$

$$\sigma_{xx} - i\tau_{xy} = \sum_{j=-N}^{M}\left[\chi_1 + \chi_2 - \chi_3 - \chi_4 + \chi_5\right]\ a_j + \left[\chi_1 - \chi_2 - \chi_3 + \chi_4 + \chi_5\right]\ b_j \tag{29}$$

$$\sigma_{yy} + i\tau_{xy} = \sum_{j=-N}^{M}\left[\chi_1 + \chi_2 + \chi_3 + \chi_4 - \chi_5\right]\ a_j + \left[\chi_1 - \chi_2 + \chi_3 - \chi_4 - \chi_5\right]b_j \tag{30}$$

where

$$\varsigma_1 = \kappa\zeta^j + \overline{\zeta}^{-j} \tag{31}$$

$$\varsigma_2 = \frac{je^{i2\theta}\,\overline{\zeta}^{\,j-1}\left[\zeta - \overline{\zeta}^{-1} + m\left(\zeta^{-1} - \overline{\zeta}\right)\right]}{1 - m\overline{\zeta}^{-2}} \tag{32}$$

$$\chi_1 = \frac{j\zeta^{j-1}}{ce^{i\theta}\left(1 - m\zeta^{-2}\right)} \tag{33}$$

$$\chi_2 = \frac{je^{i\theta}\,\overline{\zeta}^{\,j-1}}{c\left(1 - m\overline{\zeta}^{-2}\right)} \tag{34}$$

$$\chi_3 = \frac{j\left(\overline{\zeta} + m\overline{\zeta}^{-1}\right)\ \left[\left(j-1\right)\zeta^{j-2} + \left(j+1\right)\zeta^{j-4}\right]}{ce^{i3\theta}\ \left(1 - m\zeta^{-2}\right)^{\,3}} \tag{35}$$

$$\chi_4 = \frac{j\zeta^{-j-1}}{ce^{i\theta}\ \left(1 - m\zeta^{-2}\right)} \tag{36}$$

$$\chi_5 = \frac{j\left[\left(\left(j-2\right) - m^2\left(j+2\right)\right)\zeta^{j-3} - mj\,\zeta^{j-5} + mj\,\zeta^{j-1}\right]}{ce^{i3\theta}\left(1 - m\zeta^{-2}\right)^{\,3}} \tag{37}$$

From Eqs (21)-(23) the special Trefftz functions $\mathbf{N}_e$ and $\mathbf{T}_e$ may be written as follows

$$\mathbf{N}_e = \frac{1}{2G}\begin{bmatrix} \mathrm{Re}U_{-N} & \cdots & \mathrm{Re}U_M & \mathrm{Re}U_{M+N+1} & \cdots & \mathrm{Re}U_{2(M+N)} \\ \mathrm{Im}U_{-N} & \cdots & \mathrm{Im}U_M & \mathrm{Im}U_{M+N+1} & \cdots & \mathrm{Im}U_{2(M+N)} \end{bmatrix} \tag{38}$$

$$\mathbf{T}_e = \begin{bmatrix} \mathrm{Re}\,S_{1,-N} & \cdots & \mathrm{Re}\,S_{1,M+N} & \mathrm{Re}\,S_{1,M+N+1} & \cdots & \mathrm{Re}\,S_{1,2(M+N)} \\ \mathrm{Re}\,S_{2,-N} & \cdots & \mathrm{Re}\,S_{2,M+N} & \mathrm{Re}\,S_{2,M+N+1} & \cdots & \mathrm{Re}\,S_{2,2(M+N)} \\ \mathrm{Im}\,S_{3,-N} & \cdots & \mathrm{Im}\,S_{3,M+N} & \mathrm{Im}\,S_{3,M+N+1} & \cdots & \mathrm{Im}\,S_{3,2(M+N)} \end{bmatrix} \tag{39}$$

where

$$U_j = \varsigma_1 - \varsigma_2 \tag{40}$$

$$U_{M+N+j} = i(\varsigma_1 + \varsigma_2) \tag{41}$$

$$S_{1,j} = \chi_1 + \chi_2 - \chi_3 - \chi_4 + \chi_5 \tag{42}$$

$$S_{1,M+N+j} = \chi_1 - \chi_2 - \chi_3 + \chi_4 + \chi_5 \tag{43}$$

$$S_{2,j} = \chi_1 + \chi_2 + \chi_3 + \chi_4 - \chi_5 \tag{44}$$

$$S_{2,M+N+j} = \chi_1 - \chi_2 + \chi_3 - \chi_4 - \chi_5 \tag{45}$$

$$S_{3,j} = \chi_3 + \chi_4 - \chi_5 \tag{46}$$

$$S_{3,M+N+j} = \chi_3 - \chi_4 - \chi_5 \tag{47}$$

In numerical implementation, it is necessary to eliminating the rigid body movement in the above expressions. For a circular hole element, one has Re $S_{1,M+N+1}$ = Re $S_{2,M+N+1}$ = Im $S_{3,M+N+1}$ = 0, the coefficient $b_1$ has to be zero, thus the number of Trefftz terms $m$ is $2(M + N) - 1$; whereas for elliptical hole element, $m$ is chosen to be $2(M + N)$ because all terms make contributions to stresses. Besides, $m$ should be approximately equal to the degrees of freedom of the element. It is clear that Piltner's recommendation on the choice of the number of special Trefftz functions can accurately represents an element with a circular hole only.

### 2.3. Frame Functions

In this paper, we use the 16- and 32-node hole elements (RHOL16 and RHOL32 for short), as shown in Fig. 3, to conduct the contact analysis.

For each side of RHOL16 element, the frame functions are of the form

$$\begin{aligned}
&\tilde{N}_1 = \frac{2}{3}\left(\tau^2 - \frac{1}{4}\right)\tau(\tau - 1),\ \tilde{N}_2 = -\frac{8}{3}\left(\tau^2 - 1\right)\tau\left(\tau - \frac{1}{2}\right),\ \tilde{N}_3 = 4\left(\tau^2 - 1\right)\left(\tau^2 - \frac{1}{4}\right),\\
&\tilde{N}_4 = -\frac{8}{3}\left(\tau^2 - 1\right)\tau\left(\tau + \frac{1}{2}\right),\ \tilde{N}_5 = \frac{2}{3}\left(\tau^2 - \frac{1}{4}\right)\tau(\tau + 1)
\end{aligned} \tag{48}$$

Analogously, for each side of RHOL32 element, the frame functions may be written as

$$\begin{aligned}
&\tilde{N}_1 = \frac{512a}{315}\left(\tau^2 - \frac{9}{16}\right)\left(\tau^2 - \frac{1}{16}\right)\tau(\tau - 1),\ \tilde{N}_2 = -\frac{4096a}{315}\left(\tau^2 - 1\right)\left(\tau^2 - \frac{1}{16}\right)\tau\left(\tau - \frac{3}{4}\right),\\
&\tilde{N}_3 = \frac{2048}{45}\left(\tau^2 - 1\right)\left(\tau^2 - \frac{9}{16}\right)\left(\tau^2 - \frac{1}{16}\right)\tau\left(\tau - \frac{1}{2}\right),\ \tilde{N}_4 = -\frac{4096a}{45}\left(\tau^2 - 1\right)\left(\tau^2 - \frac{9}{16}\right)\tau\left(\tau - \frac{1}{4}\right)\\
&\tilde{N}_5 = \frac{1024a}{9}\left(\tau^2 - 1\right)\left(\tau^2 - \frac{9}{16}\right)\left(\tau - \frac{1}{16}\right),\ \tilde{N}_6 = -\frac{4096a}{45}\left(\tau^2 - 1\right)\left(\tau^2 - \frac{9}{16}\right)\tau\left(\tau + \frac{1}{4}\right),\\
&\tilde{N}_7 = \frac{2048}{45}\left(\tau^2 - 1\right)\left(\tau^2 - \frac{9}{16}\right)\left(\tau^2 - \frac{1}{16}\right)\tau\left(\tau + \frac{1}{2}\right),\ \tilde{N}_8 = -\frac{4096a}{315}\left(\tau^2 - 1\right)\left(\tau^2 - \frac{1}{16}\right)\tau\left(\tau + \frac{3}{4}\right)\\
&\tilde{N}_9 = \frac{512a}{315}\left(\tau^2 - \frac{9}{16}\right)\left(\tau^2 - \frac{1}{16}\right)\tau(\tau + 1)
\end{aligned} \tag{49}$$

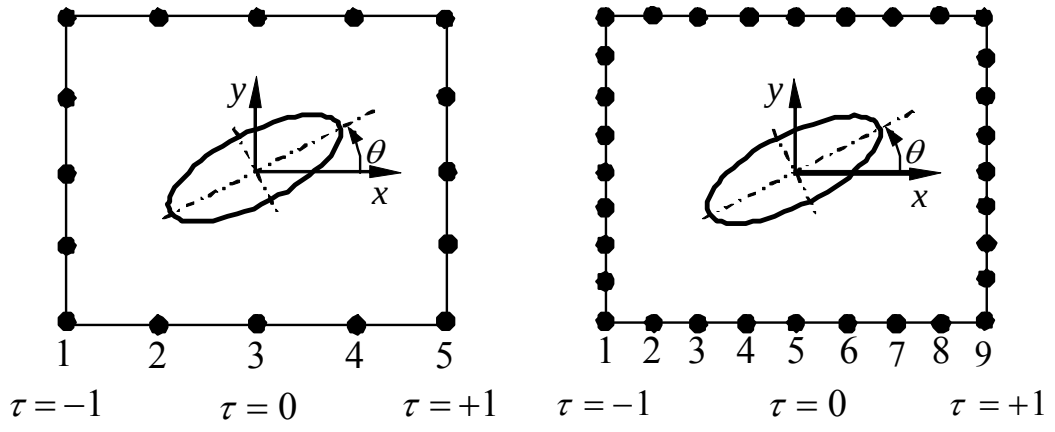


**Figure 3: New Special Purpose Hole Element**

## 3. DISCUSSION OF RESULTS

As shown in Fig. 4, an elastic rectangular punch pressed on an elastic foundation with a hole or holes is considered to assess the performance of the proposed special purpose element model. The upper surface of the punch is subjected to a uniform pressure $q$ = 1.2MPa in the vertical direction. The same material properties characterized by Young's modulus of 4000MPa and Poisson's ratio of 0.35 are assumed for both bodies. In our contact analysis, the plane stain state is assumed and the direct constraint-Trefftz FEM is used [9]. Both 4-node regular Trefftz plane element (C2D4T) [9] and RHOL16 or RHOL32 element are employed to discrete the bodies in contact. C2D4T is used to model regular element (elements without hole); while RHOL16 or RHOL32 is used to model hole element.

The influence of holes on the contact pressure distribution has been examined from the following five aspects:

(1) Radius ($r$) of circular hole
(2) Position of circular hole
(3) Direction angle ($\theta$) of elliptical hole
(4) Ratio of semi-minor to semi-mojor axes ($b/a$) of elliptical hole
(5) Multiple holes

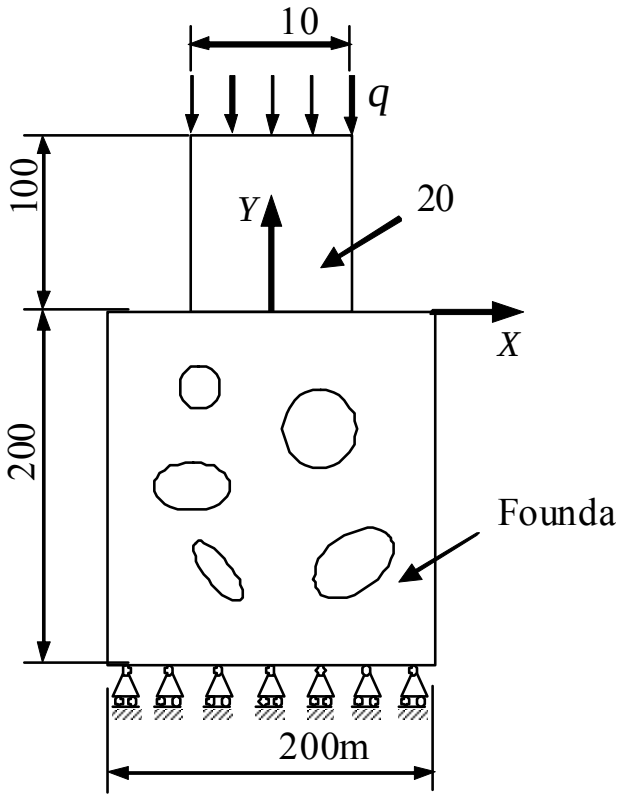


**Figure 4: Configuration of the Test Problem**

Let us first analyze the effect of radius of a circular hole. Here a range of radii $r$ = 4, 6, 8, 10mm is considered. The foundation with one individual circular hole, whose center locates at (0, -20mm), is partitioned into 264 C2D4T elements and one 20mm$\times$20mm RHOL16 element (Fig. 5a). The same boundary value problem is analyzed by ABAQUS and corresponding mesh for four kinds of radii is shown in Fig. 5(b-e), in which 783, 769, 760 and 687 (ABAQUS Element CPE4H) elements are respectively used. It can be seen that use of special hole element leads to significant reduction in the number of elements as well as the total degrees of freedom. As shown in Fig. 6, the same contact pressure distribution for a range of radii of circular holes, caused by a uniform load, are obtained using the coarse HT FE mesh without sacrificing accuracy. This clearly demonstrates the efficiency of the proposed special purpose element model. Furthermore, as the radius becomes larger, the contact pressure shows a marked decrease within $|X| < 13.8$mm while opposite trend occurs within 13.8mm $<|X|<$ 45 mm. However, the contact pressure at

$|X|$ = 13.8mm, 50 mm is hardly affected. For the case of $r$ = 10mm, the contact pressure dropped approximately by 43.21% compared to the model without holes.

Next, effects of the position of a hole embedded in the contacted body on contact pressure distribution is investigated. In this example, a circular hole with radius of 8mm moving in horizontal ($X_0$ = 0, $Y_0$ = 20, 30, 40, 50mm) or vertical direction ($X_0$ = 0, 25, 50mm, $Y_0$ = –20mm), is analyzed. $X_0$, $Y_0$ are coordinates of the center of the hole. The meshes are shown in Fig. 7. It is observed from Fig. 8 that the numerical results for four distinct vertical positions coincide with the predictions by ABAQUS. Furthermore, as the hole moves far away from the interface region the contact pressure distribution slightly varies. It is predicted that if the foundation becomes large and the hole keeps far away from the interface sufficiently, the results will tend to those without holes. For the horizontal position variation (Fig. 9), as the hole moves towards the right side minimum of contact pressure shifts in the same direction and becomes remarkable larger.

The new hole element remedies the deficiency of Piltner's element which has some difficulty in dealing with the structure with elliptical holes in arbitrary direction (Fig. 10). Now, we will investigate the effect of the direction angle (θ) of an elliptical hole on the contact pressure distribution using this new element. As shown in Fig. 10, we consider the contact between the punch and the foundation with an elliptical hole whose center locates at (0, -60mm). The foundation is discretized into 196 C2D4T elements and 1 50mm × 50mm RHOL32 elliptical hole element (246 nodes). The contact pressure distribution for various direction angles is plotted in Fig. 11. It can be seen that the value of θ affects significantly the contact behavior, especially the contact pressure distribution. An elliptical hole with a horizontal direction θ = 0° generates a pressure distribution a bit far from that with a non-horizontal one.

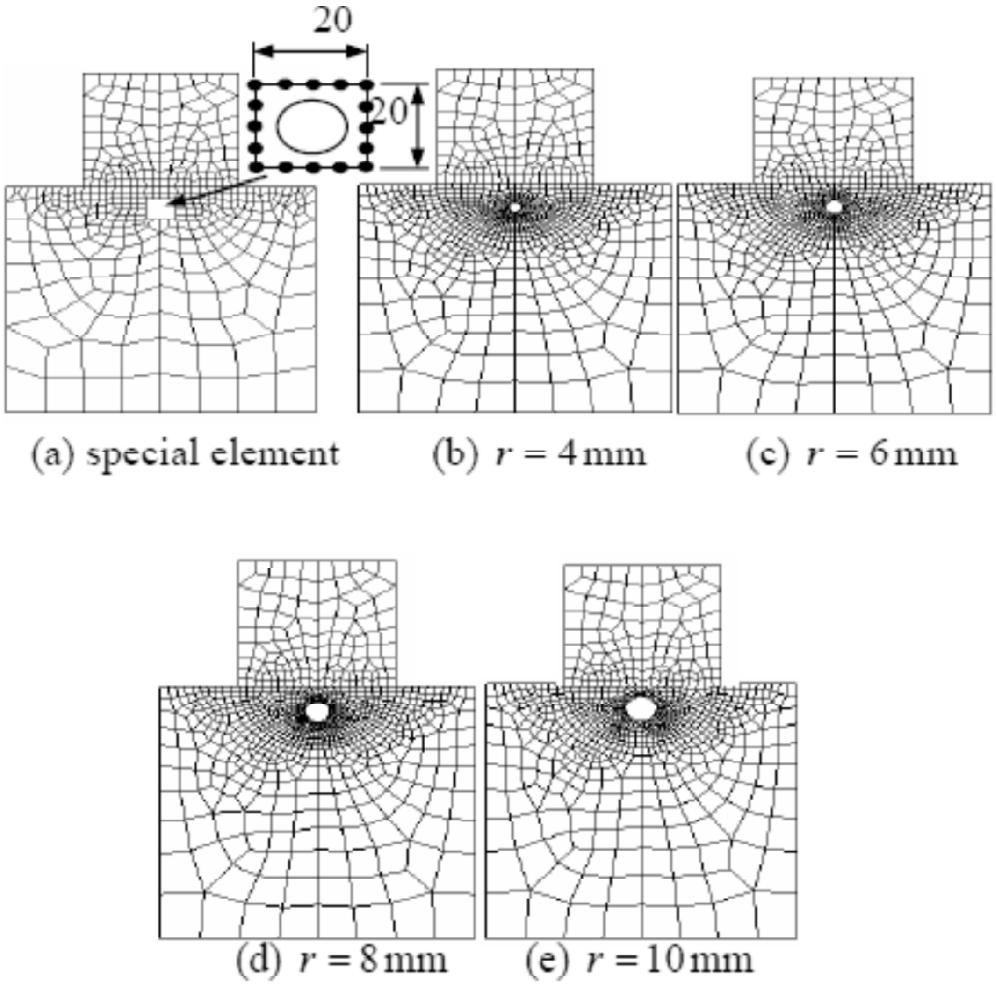


**Figure 5: Element Meshes**

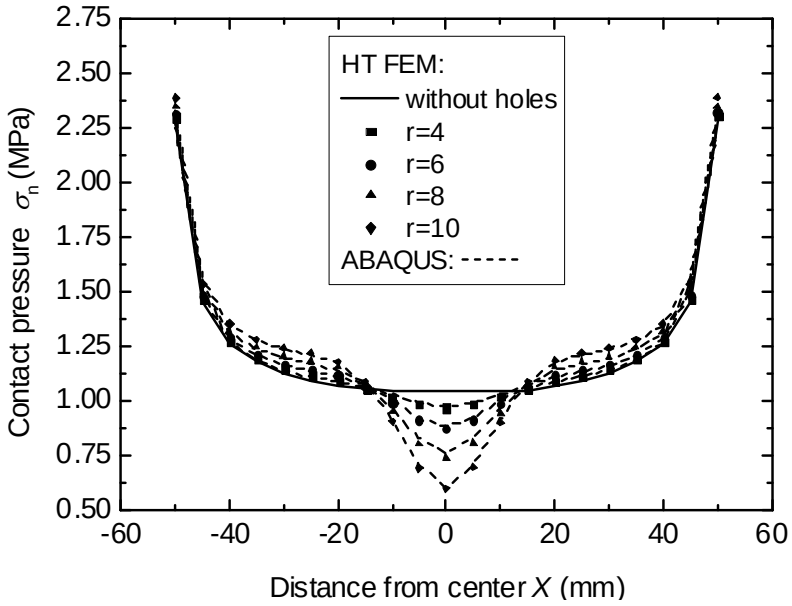


**Figure 6: Effect of Radius on the Contact Pressure Distribution**

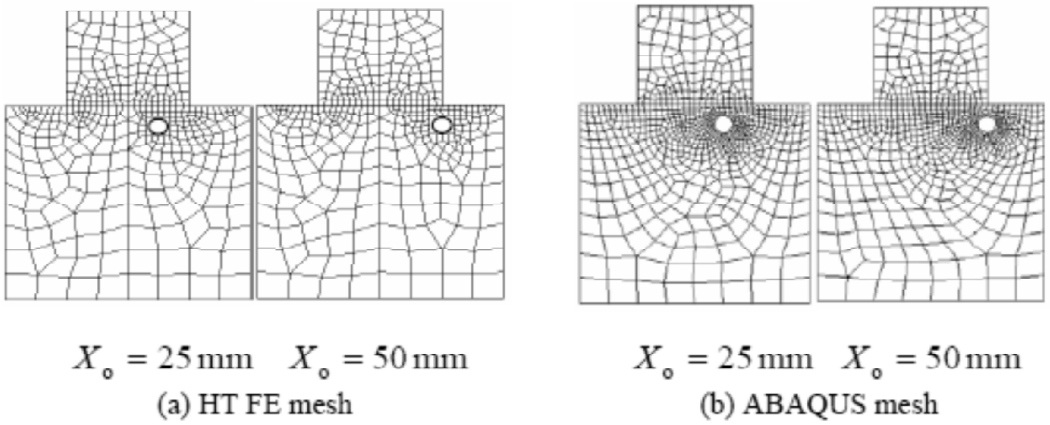


**Figure 7: HT FE and ABAQUS Meshes for the Hole at Different Horizontal Position**

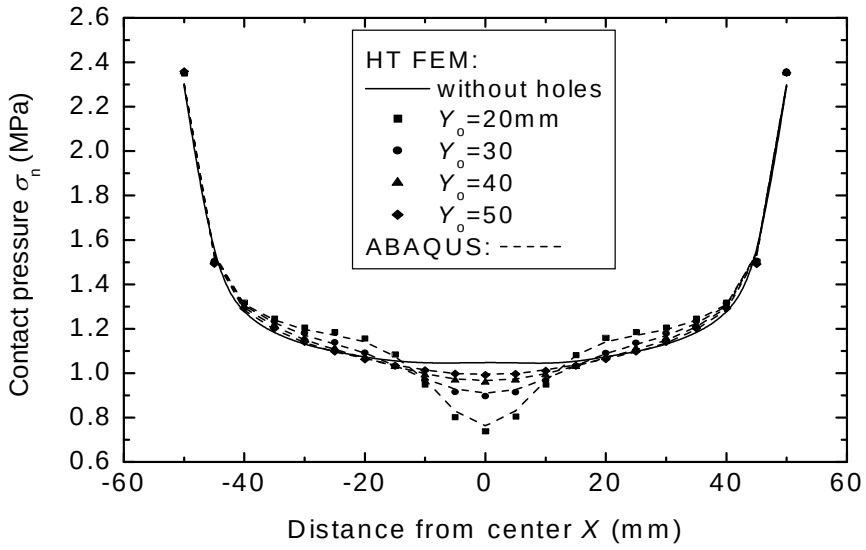


**Figure 8: Effect of the Vertical Position of the Hole on the Contact Pressure Distribution**

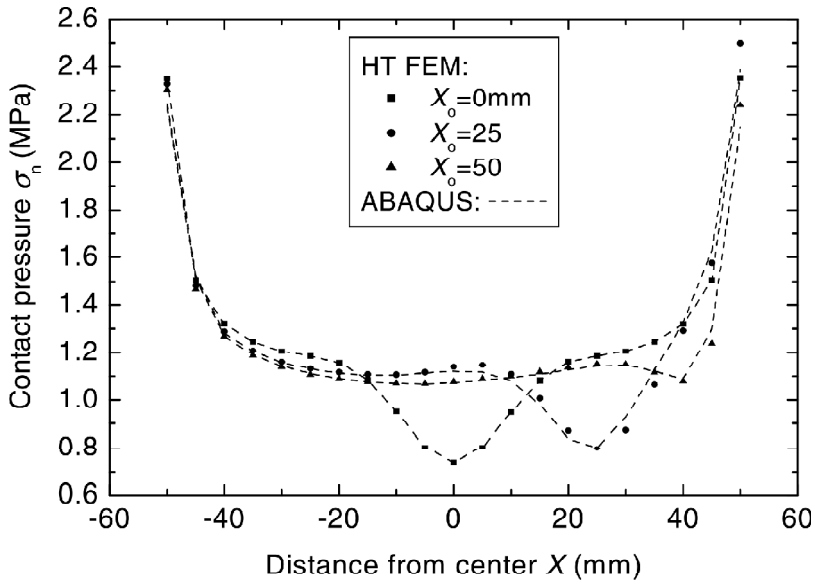


**Figure 9: Effect of the Horizontal Position of the Hole on the Contact Pressure Distribution**

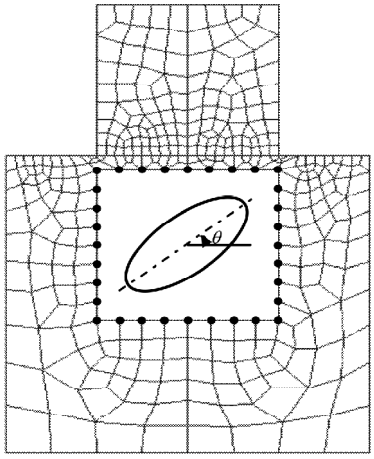


**Figure 10: Element Mesh for the Ellipitical Hole with Direction Angle θ**

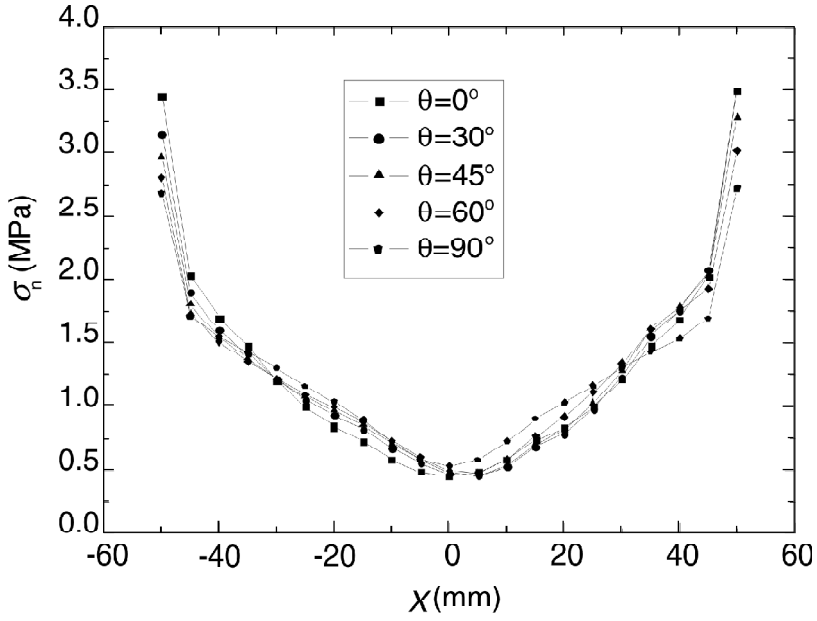


**Figure 11: Effect of a Direction Angle (θ) of the Elliptical Hole on the Contact Pressure Distribution**

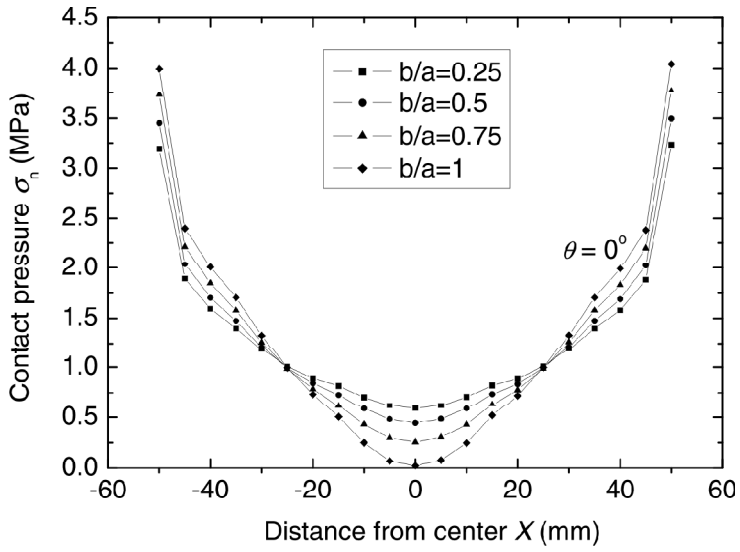


**Figure 12: Effect of a Ratio (*b* / *a*) on the Contact Pressure Distribution for θ = 0°**

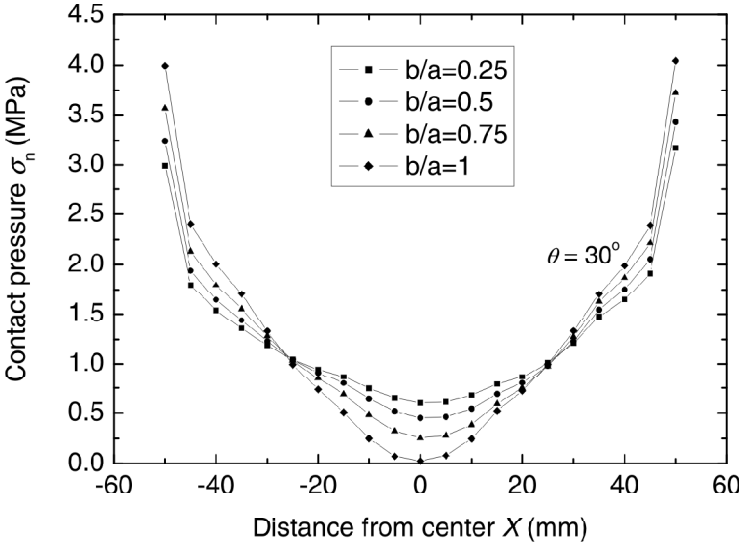


**Figure 13: Effect of a Ratio (*b* / *a*) on the Contact Pressure Distribution for θ = 30°**

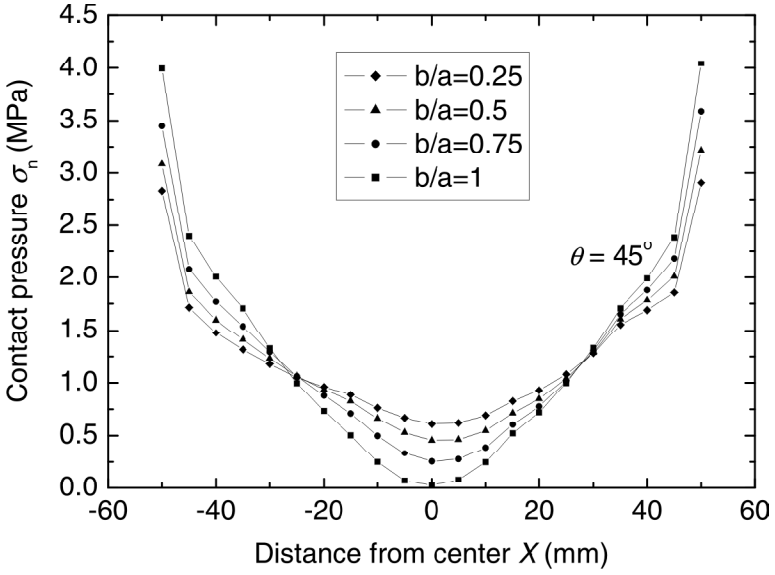


**Figure 14: Effect of a Ratio (*b* / *a*) on the Contact Pressure Distribution for θ = 45°**

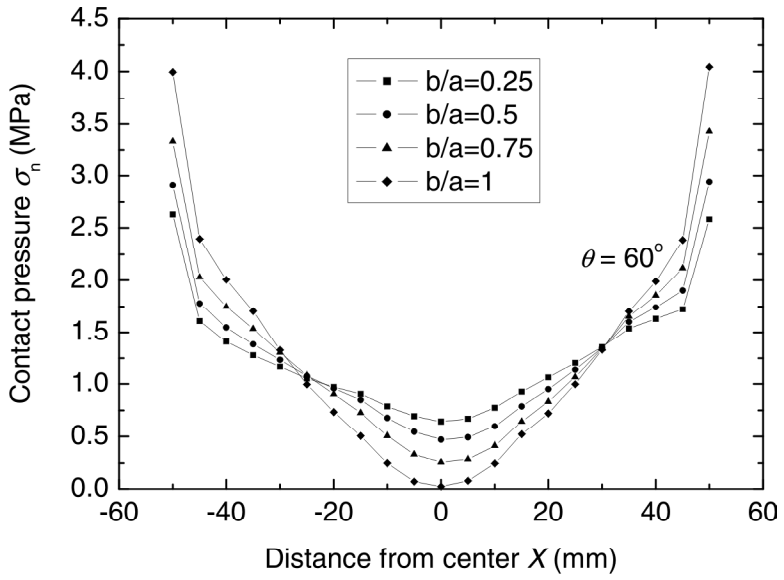


**Figure 15: Effect of the Ratio (*b* / *a*) on the Contact Pressure Distribution for θ = 60°**

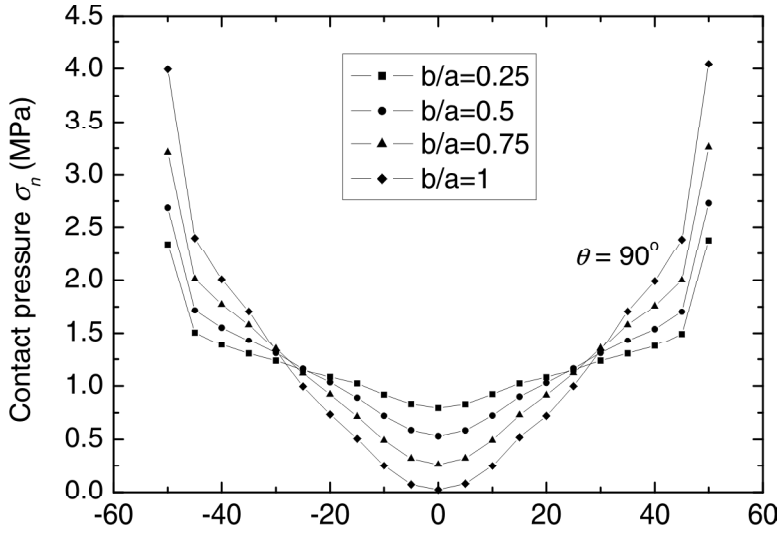


**Figure 16: Effect of the Ratio (*b* / *a*) on the Contact Pressure Distribution for θ = 90°**

For the contact model with an elliptical hole, the ratio of the semi-major to the semi-minor (*b* / *a*) also has an effect on the contact pressure distribution. In order to study this case, the same HT FE mesh as given in Fig. 10, where the elliptical hole with distinct ratios ranging from 0.25 to 1.0 is chosen, is used. Figs. 12 to 16 show the numerical results for five direction angles. Obviously, the effect of *b* / *a* on the contact pressure distribution may be partitioned into three sub-regions: increase, constant and decrease. Within the increase sub-region, as *b* / *a* grows the contact pressure increases, whilst within the decrease sub-region, the inverse phenomenon occurs. For the constant sub-region there is little or no effect by the aspect ratio *b* / *a*. The bound for each sub-region is given in Table 1.

**Table 1**
**Three Affected Sub-regions for Various Direction Angles**

| *θ(deg.)* | *Increase sub- region (mm)* | *Constant sub-region (mm)* | *Decrease sub-region (mm)* |
|---|---|---|---|
| 0 | $\|X\|>25$ | $\|X\|=25$ | $\|X\|<25$ |
| 30 | $-26.4<X<25$ | $X=-26.4$, $X=25$ | $X<-26.4$, $X>25$ |
| 45 | $-26.5<X<28.5$ | $X=-26.5$, $X=28.5$ | $X<-26.5$, $X>28.5$ |
| 60 | $-26.3<X<30.9$ | $X=-26.3$, $X=30.9$ | $X<-26.3$, $X>30.9$ |
| 90 | $-28.4<X<28$ | $X=-28.4$, $X=28$ | $X<-28.4$, $X>28$ |

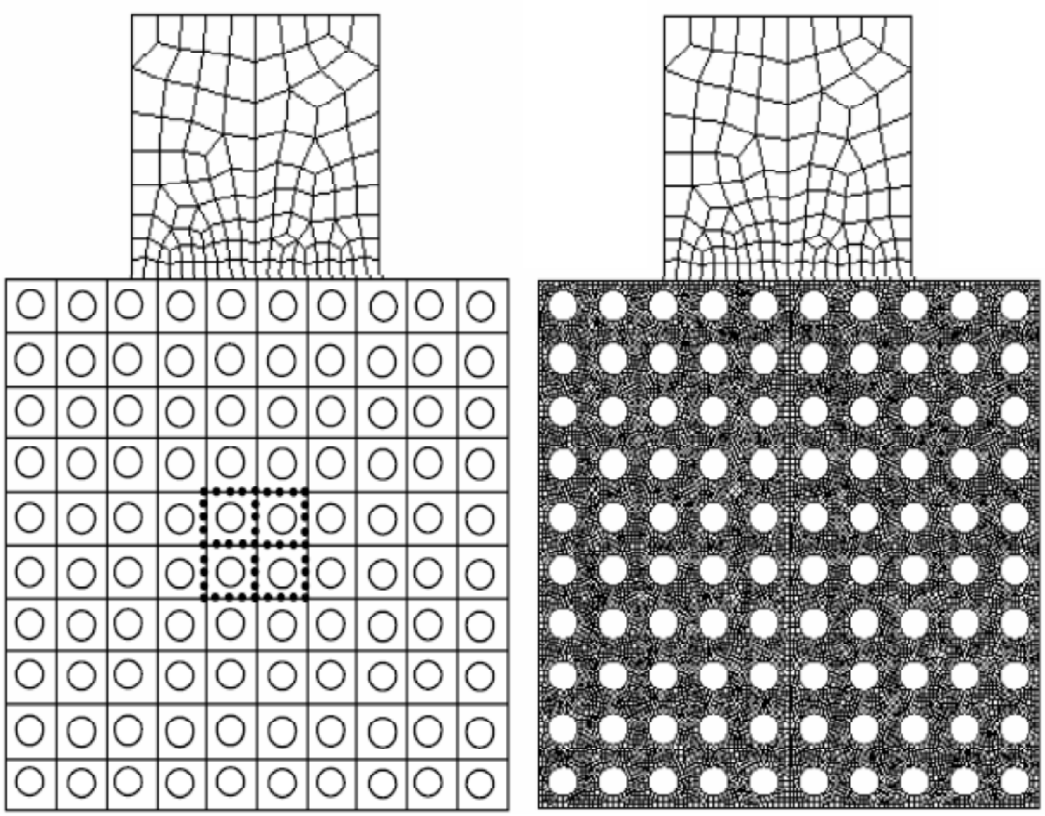

(a) HT FE mesh (b) ABAQUS mesh

**Figure 17: Multiple Hole Problem**

Finally, we investigate the case of the foundation with 100 identical circular holes whose radii is 6mm. As shown in Fig. 17(a), the foundation consists of 100 (20mm × 20mm) RHOL16 circular hole elements (781 nodes). The corresponding conventional mesh with 10741 CPE4H elements (11842 nodes) is obtained using ABAQUS (Fig. 17b), Fig. 18 shows the contact pressure distribution. The comparison demonstrates that the results predicted by HT FEM and ABAQUS accord approximately with each other except for the two singular points. This discrepancy is mainly due to less discrete nodes by HT FEM than by ABAQUS along the surface of the foundation.

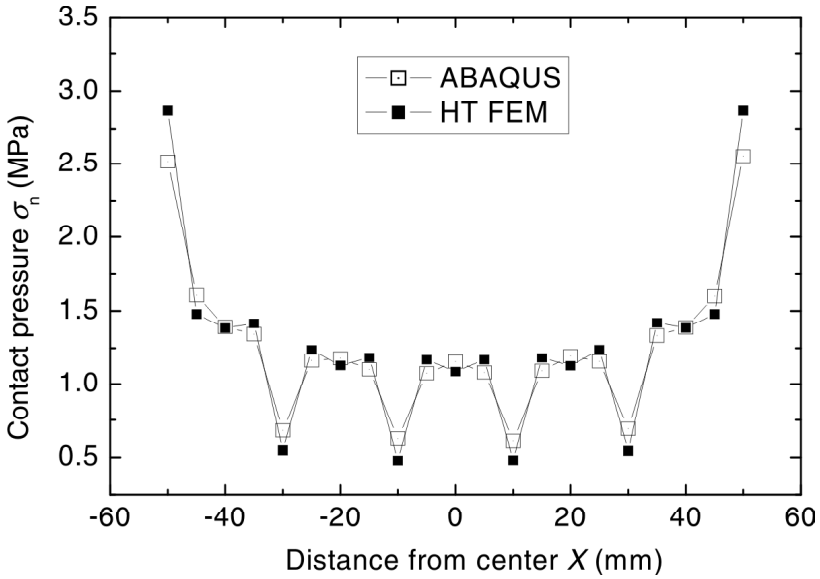


**Figure 18: Effect of Multiple Holes on the Contact Pressure Distribution**

## 4. CONCLUSIONS

A novel Trefftz hole element, based on the work of Piltner [4], is developed by introducing a rotated mapping function and using different terms of special Trefftz functions. This element can treat the structure with an elliptical hole in arbitrary direction without any difficulty. Using the proposed hole element and the direct constraint technique[9], the contact pressure distributions along the interface between an elastic rectangular punch and an elastic foundation with holes are investigated.. Compared with the conventional FEM (ABAQUS), HT FEM can accurately simulate the mechanical behavior around a hole without troublesome mesh refinement locally. This demonstrates the efficiency of the novel Trefftz hole element in the present study. Also, comparisons of the results with ABAQUS models and HT FE analyses have generally shown good agreement, although inaccuracies in some numerical simulations have been observed.

The study presents a parametric investigation of the contact behavior of a punch and a foundation with holes. We note that the larger the radius of a circular hole embedded in the foundation and the closer the distance from the center of a hole to the contact interface, the more remarkable the effect of holes on the contact pressure distribution. Moreover, an elliptical hole with a horizontal direction angle generates a pressure distribution a bit far from that with a non-horizontal one. The ratio of semi-major axis to semi-minor axis affects the contact pressure, producing three remarked sub-regions.

The present work can be extended to study elastic contact problems with multiple holes randomly dispersed within one or both contacting bodies. In the meantime, the extension to frictional cases is also possible.

### *References*

[1] Jirousek, J. and Leon, N., "A Powerful Finite Element for Plate Bending", *Comp. Meth. Appl. Mech. Engrg.*, **12**, 77-96, (1977).

[2] Qin, Q. H., The Trefftz Finite and Boundary Element Method, WIT Press, Southampton (2000).

[3] Qin, Q. H., "Trefftz Finite Element Method and its Applications", *Appl. Mech. Reviews*, **58**, 316-337, (2005).

[4] Piltner, P., "Special Finite Elements with Holes and Internal Cracks", *Int. J. Numer. Meth. Engng.*, **21**, 1471-1485, (1985).

[5] Zhao, J. P. and Shan, H. Z., "Stress Analysis Around Holes in Orthotropic Plates by the Subregion Mixed Finite Element Method", *Comput. Struct.*, **41**, 105-108, (1991).

[6] Chen, H. C., "Special Finite Elements Including Stress Concentration Effects of a Hole", *Finite Elem. Ana. Des.*, **13**, 249-258, (1993).

[7] ZieliDski, A. P., "Special Trefftz Elements and Improvement of their Conditioning", *Communi. Numer. Meth. Eng.*, **13**, 765-775, (1997).

[8] Zeng, D., Kartsube, N. and Zhang, J., "A Hybrid Finite Element Method for Fluid-filled Porous Materials", *Int. J. Numer. Anal. Meth. Geomech.*, **23**, 1521-1534, (1999).

[9] Wang, K. Y., Qin, Q. H., Kang, Y. L., Wang, J. S. and Qu, C. Y., "A Direct Constraint-Trefftz FEM for Analyzing Elastic Contact Problems", *Int. J. Numer. Meth. Eng.*, **63**, 1694-1718, (2005).

[10] Muskhelishvili, N. I., Some Basic Problems of the Mathematical Theory of Elasticity, Noordhoff, Groningen, Holland (1953).